in the table, as well as the root-mean-square error 0.5353 of integer approximation.

For the inverse integer DFT, the additional control bits $(\alpha_9, \alpha_{10}, \alpha_{11}, \alpha_{12})$ are calculated on the next stage.

Stage 4 (Additional Four Control Bits): The second and fourth components of the eight-point paired transform are equal to $(-3+j)-(-1-3j)=-2+4j$ and $-j-(-6-3j)=6+2j$, respectively. The complex number $-2+4j$ is transformed by C_2 as follows:

$$\mathcal{A}_{0.7071}:(-2+4)=2\rightarrow\begin{cases}\vartheta_0(2)=1\\ \alpha_9=1\end{cases}$$
$$\mathcal{A}_{0.7071}:(4-(-2))=6\rightarrow\begin{cases}\vartheta_0(6)=4\\ \alpha_{10}=1\end{cases}$$

and therefore $\mathcal{C}_2(-2+4j)=\vartheta_0(2)+j\,\vartheta_0(6)=1+4j$. However, we need only two control bits $\alpha_9=1$ and $\alpha_{10}=1$. The remaining two control bits are calculated similarly from the integer approximation $C_6(6+2j)$:

$$\mathcal{A}_{0.7071}:(6-2)=4\rightarrow\begin{cases}\vartheta_0(4)=3\\ \alpha_{11}=0\end{cases}$$
$$\mathcal{A}_{0.7071}:(6+2)=8\rightarrow\begin{cases}\vartheta_0(8)=6\\ \alpha_{12}=0.\end{cases}$$

Thus the additional four control bits are 1, 1, 0, and 0.

We now consider for comparison the application of the three-step lifting schemes [5], [6] for integer approximation of two rotations which represent multiplications by factors W^2 and W^6, instead of the multiplications $\mathcal{C}_2$ and $\mathcal{C}_6$ with control bits. Each integer lifting scheme requires three multiplications instead of two multiplications when using two integer transforms $\mathcal{A}_{0.7071}$.

Stage 4 (Lifting Scheme): The first output of the eight-point paired transform is calculated as $(-7)-(j)=-7-j$ and the third output $(-2+2j)-(-2-2j)=4j$. The integer approximations of multiplication of complex numbers $-2+4j$ and $6+2j$ by the factors W^2 and W^6, are calculated, respectively, as

$$(-2+4j)\cdot W^2\rightarrow\begin{array}{|c|c|c|}\hline \mathcal{Q} & -0.7071 & \mathcal{Q}\\ \hline 0.4142 & \mathcal{Q} & 0.4142\\ \hline\end{array}\circ\begin{bmatrix}-2\\4\end{bmatrix}=\begin{bmatrix}2\\4\end{bmatrix}$$

and

$$(6+2j)\cdot W^6\rightarrow\begin{array}{|c|c|c|}\hline \mathcal{Q} & -0.7071 & \mathcal{Q}\\ \hline 2.4142 & \mathcal{Q} & 2.4142\\ \hline\end{array}\circ\begin{bmatrix}6\\2\end{bmatrix}=\begin{bmatrix}-3\\-6\end{bmatrix}.$$

Here, the quantizing operation is the rounding, i.e., $\mathcal{Q}(x)=[x]$. Using the obtained numbers $2+4j$ and $-3-6j$ together with other inputs $-7-j$ and 4, we obtain the following components of the 16-point integer DFT at frequency-points 3, 7, 11, and 15: $F_{15}=-21+4j$, $F_7=-1-6j$, $F_{11}=-2+j$, and $F_3=-4-3j$. These values are shown in the last column of Table I for the 16-point integer DFT with two lifting schemes. The root-mean-square error of integer approximation by lifting schemes equals 0.5812. The property of complex conjugate of the transform components F_p and F_{8-p}, $p=3, 7$, does not hold for the integer approximation of the 16-point DFT by the lifting schemes.

IV. Conclusion

The integer approximation of the 16-point discrete Fourier transform with twelve control bits has been described for the case of real inputs. The block-diagrams of the forward and inverse transforms have been discussed in detail. This approximation uses 16 operations of real multiplication and 62 additions. The implementation of the three-lifting schemes in the paired algorithm, which requires two more multiplications, has also been presented.

References

[1] A. M. Grigoryan, "Novel reversible integer Fourier transform with control bits," *IEEE Trans. Signal Process.*, vol. 55, no. 11, pp. 5267–5276, Nov. 2007.

[2] A. M. Grigoryan, "2-D and 1-D multi-paired transforms: Frequency-time type wavelets," *IEEE Trans. Signal Process.*, vol. 49, no. 2, pp. 344–353, Feb. 2001.

[3] A. M. Grigoryan and S. S. Agaian, *Multidimensional Discrete Unitary Transforms: Representation, Partitioning and Algorithms*. New York: Marcel Dekker, 2003.

[4] A. M. Grigoryan and V. S. Bhamidipati, "Method of flow graph simplification for the 16-point discrete Fourier transform," *IEEE Trans. Signal Process.*, vol. 53, no. 1, pp. 384–389, Jan. 2005.

[5] R. Calderbank, I. Daubechies, W. Sweldens, and B.-L. Yeo, "Wavelet transforms that map integers to integers," *Appl. Comput. Harmon. Anal.*, vol. 5, no. 3, pp. 332–369, 1998.

[6] S. Oraintara, Y.-J. Chen, and T. Q. Nguyen, "Integer fast Fourier algorithms," *IEEE Trans. Signal Process.*, vol. 50, no. 3, pp. 607–618, Mar. 2002.

Accuracy Comparison of LS and Squared-Range LS for Source Localization

Erik G. Larsson and Danyo Danev

***Abstract*—In this correspondence, we compute a closed-form expression for the asymptotic (large-sample) accuracy of the recently proposed squared-range least-squares (SR-LS) method for source localization [A. Beck, P. Stoica, and J. Li, "Exact and approximate solutions of source localization problems," *IEEE Trans. Signal Process.*, vol. 56, no. 5, pp. 1770–1778, May 2008]. We compare its accuracy to that of the classical least-squares (LS) method and show that LS and SR-LS perform differently in general. We identify geometries where the performances of the methods are identical but also geometries when the difference in performance is unbounded.**

***Index Terms*—Least squares methods, position measurement, signal analysis.**

I. Introduction, Model, and Problem Formulation

Source localization is important in many applications, for example, GPS [2], positioning of mobile phones [3], [4] and localization of nodes in a sensor network [5]. We consider the problem of source-localization in two dimensions, using absolute range measurements. Specifically,

Manuscript received April 14, 2009; accepted August 26, 2009. First published September 09, 2009; current version published January 13, 2010. The associate editor coordinating the review of this manuscript and approving it for publication was Prof. Olivier Besson. This work was supported in part by the Swedish Research Council (VR), the Swedish Foundation of Strategic Research (SSF), and the CENIIT foundation. E. Larsson is a Royal Swedish Academy of Sciences (KVA) Research Fellow supported by a grant from the Knut and Alice Wallenberg Foundation.

The authors are with the Department of Electrical Engineering (ISY), Linköping University, SE-581 83 Linköping, Sweden (e-mail: egl@isy.liu.se; danyo@isy.liu.se).

Digital Object Identifier 10.1109/TSP.2009.2032036

the task is to determine the position of a source node $\mathcal{S}$ located at the coordinates $(x_0, y_0) \in \mathbb{R}^2$, from a set of noisy distance measurements to M anchors $\mathcal{A}_1, \ldots, \mathcal{A}_M$. Anchor $\mathcal{A}_m$ is located at $(x_m, y_m) \in \mathbb{R}^2$, $m = 1, \ldots, M$. For future use, let us call the set of anchors $\mathcal{A} \triangleq \{\mathcal{A}_1, \ldots, \mathcal{A}_M\}$. The true distance between $\mathcal{S}$ and $\mathcal{A}_m$ is

$$d_m \triangleq \sqrt{(x_0 - x_m)^2 + (y_0 - y_m)^2}.$$

We assume that N independent measurements $r_{m,n}$ of each distance d_m are available

$$\begin{aligned} r_{m,n} &= d_m + e_{m,n} \\ &= \sqrt{(x_0 - x_m)^2 + (y_0 - y_m)^2} + e_{m,n}, \end{aligned}$$

$n = 1, \ldots, N$, where $e_{m,n}$ are measurement errors.

We are interested in the asymptotic (large N) behavior of two specific source localization methods, namely the classical least-squares (LS) [6], [7] and the more recently proposed squared-range least-squares (SR-LS) method [1]. LS is well known and estimates the position by a straightforward least-squares fit:

$$(\hat{x}_{\mathrm{LS}}, \hat{y}_{\mathrm{LS}}) = \arg\min_{x,y} \sum_{n=1}^{N} \sum_{m=1}^{M} \times \left(r_{m,n} - \sqrt{(x - x_m)^2 + (y - y_m)^2} \right)^2.$$

It is not hard to show that finding the point $(\hat{x}_{\mathrm{LS}}, \hat{y}_{\mathrm{LS}})$ is equivalent to minimizing

$$f_{\mathrm{LS}}(x, y) \triangleq \sum_{m=1}^{M} \left(r_m - \sqrt{(x - x_m)^2 + (y - y_m)^2} \right)^2 \qquad (1)$$

with respect to x and y, where we have defined the averaged measurements

$$r_m \triangleq \frac{1}{N} \sum_{n=1}^{N} r_{m,n} = \sqrt{(x_0 - x_m)^2 + (y_0 - y_m)^2} + e_m. \qquad (2)$$

In (2), $e_m \triangleq 1/N \sum_{n=1}^{N} e_{m,n}$ is averaged noise. LS is equivalent to maximum-likelihood (ML) if $e_{m,n}$ are independent identically distributed (i.i.d.) zero-mean Gaussian. This implies that LS achieves the Cramér–Rao bound (CRB) on the achievable accuracy, when N is large [6]. LS comes with an important drawback, however. The function $f_{\mathrm{LS}}(x, y)$ is nonconvex, and it is therefore difficult to minimize.

Recently, Beck *et al.* [1] proposed an alternative localization method, SR-LS, that is based on squaring all measurements before the least-squares fit takes place. More precisely, the SR-LS method forms a position estimate $(\hat{x}_{\text{SR-LS}}, \hat{y}_{\text{SR-LS}})$ by minimizing the following function with respect to x and y:

$$f_{\text{SR-LS}}(x, y) \triangleq \sum_{m=1}^{M} \left(r_m^2 - \left((x - x_m)^2 + (y - y_m)^2 \right) \right)^2. \qquad (3)$$

For $M = 2$, LS and SR-LS are equivalent in all cases of practical interest because then, an (x, y) can be found for which $f_{\mathrm{LS}}(x, y) = f_{\text{SR-LS}}(x, y) = 0$. This corresponds to finding the intersection point(s) between two circles, provided that the circles do intersect.[1] For $M > 2$, LS and SR-LS are not equivalent. In particular, SR-LS is suboptimal in the ML sense if $e_{m,n}$ are Gaussian. SR-LS however, has another exceptionally attractive advantage over LS: the global minimum of $f_{\text{SR-LS}}(\cdot)$ can be found exactly, using standard (yet sophisticated) optimization tools [1]. The question that remains, however, is how much accuracy is lost when using SR-LS instead of LS. To some extent this question was addressed in [1]. However, the performance investigations therein were limited to simulations of specific scenarios from which it is hard to draw general conclusions. In this correspondence, we compute the asymptotic (large N) accuracies of LS and SR-LS in closed form and compare them.

To facilitate the analysis, we will assume that the errors $e_{m,n}$ are independent with zero mean, variances $E[e_{m,n}^2] = \sigma^2$, zero third-order moment, and bounded fourth-order moment $E[e_{m,n}^4] = \alpha\sigma^4$, for some constant α.[2] This is satisfied for most symmetric distributions of interest, those from the exponential family in particular. For example, for Gaussian measurements errors we have $\alpha = 3$. We do not make any further assumptions on $e_{m,n}$. Under these assumptions we have for e_m in (2):

$$\begin{aligned} E[e_m] &= 0, \quad E[e_m^2] = \frac{\sigma^2}{N}, \\ E[e_m^4] &= \frac{\sigma^4}{N^2} \left(3 + \frac{\alpha - 3}{N} \right). \end{aligned}$$

Finally, for notational convenience, but without loss of generality, from now on we will assume that the true location of $\mathcal{S}$ is $(x_0, y_0) = (0, 0)$.

II. Preliminaries: Asymptotic Analysis Tools

We briefly recapture some basic facts about large-sample analysis in nonlinear estimation. See, e.g., [8]–[10] for a detailed treatment. The task at hand is to determine the asymptotic (large N, fixed σ^2, and fixed M) statistics of the location estimates $(\hat{x}, \hat{y})$ obtained by minimizing (1) and (3), respectively. The standard way to carry out this type of analysis is to compute the curvature of the cost function locally around its minimum, typically by approximating it with a quadratic function. More precisely, let

$$\begin{aligned} \boldsymbol{f}' &\triangleq \begin{bmatrix} \frac{\partial f}{\partial x}(0,0) \\ \frac{\partial f}{\partial y}(0,0) \end{bmatrix}, \\ \boldsymbol{F}'' &\triangleq \begin{bmatrix} \frac{\partial^2 f}{\partial x^2}(0,0) & \frac{\partial^2 f}{\partial x \partial y}(0,0) \\ \frac{\partial^2 f}{\partial x \partial y}(0,0) & \frac{\partial^2 f}{\partial y^2}(0,0) \end{bmatrix} \end{aligned}$$

be the gradient and the Hessian of $f(\cdot)$ evaluated at the true location $(x, y) = (0, 0)$ and define

$$\bar{\boldsymbol{F}}'' = \lim_{N \to \infty} \boldsymbol{F}''.$$

Then, provided that $\boldsymbol{F}''$ is continuous and that the estimate $(\hat{x}, \hat{y})$ is consistent, i.e., $(\hat{x}, \hat{y}) \to (0, 0)$ as $N \to \infty$, we have that for N large, $(\hat{x}, \hat{y}) \sim N(\boldsymbol{0}, \boldsymbol{Q})$, where

$$\boldsymbol{Q} \triangleq (\bar{\boldsymbol{F}}'')^{-1} E[\boldsymbol{f}' \boldsymbol{f}'^T] (\bar{\boldsymbol{F}}'')^{-1}. \qquad (4)$$

Both LS and SR-LS are consistent, because when $N \to \infty$, both $f_{\mathrm{LS}}(x, y)$ and $f_{\text{SR-LS}}(x, y)$ converge uniformly to functions that have a unique global minimum at $(0, 0)$. (Recall footnote 1 about ambiguities.) More precisely,

$$\sup_{(x,y) \in \Omega} |f_{\mathrm{LS}}(x, y) - f_{\mathrm{LS}}^{\infty}(x, y)| \to 0$$

[1] Throughout the paper, we shall assume than any ambiguities (non-unique global minimum of $f(x, y)$) can be resolved.

[2] At some expense in notation, the accuracy analysis presented in what follows can be extended to the case when $e_{m,n}$ have different variances. In this case, weights need to be introduced into the cost functions (1) and (3).

and

$$\sup_{(x,y)\in\Omega} |f_{\text{SR-LS}}(x,y) - f^{\infty}_{\text{SR-LS}}(x,y)| \to 0$$

when $N \to \infty$ for any compact set Ω, where

$$f^{\infty}_{\text{LS}}(x,y) \triangleq \sum_{m=1}^{M} \left(\sqrt{x_m^2+y_m^2} - \sqrt{(x-x_m)^2+(y-y_m)^2}\right)^2,$$
$$f^{\infty}_{\text{SR-LS}}(x,y) \triangleq \sum_{m=1}^{M} \left((x_m^2+y_m^2) - ((x-x_m)^2+(y-y_m)^2)\right)^2. \quad (5)$$

To show this convergence, we use the fact that $e_{m,n}$ are i.i.d. with finite variances, and the law of large numbers [11, p. 213] to establish that

$$\lim_{N\to\infty} r_m = \sqrt{x_m^2+y_m^2}. \quad (6)$$

Since the convergence is uniform and $f^{\infty}_{\text{LS}}(x,y)$ and $f^{\infty}_{\text{SR-LS}}(x,y)$ have unique minima at $(0,0)$, it follows that $(\hat{x}_{\text{LS}}, \hat{y}_{\text{LS}}) \to (0,0)$ and $(\hat{x}_{\text{SR-LS}}, \hat{y}_{\text{SR-LS}}) \to (0,0)$ as $N \to \infty$ (see, e.g., [10, Exercise 7.15]). Furthermore, both $f_{\text{LS}}(x,y)$ and $f_{\text{SR-LS}}(x,y)$ are continuously differentiable an arbitrary number of times. In particular, $\boldsymbol{F}''$ is continuous.

Hence, to carry out the analysis, we need to determine the 2×2 matrices $E[\boldsymbol{f}'\boldsymbol{f}'^T]$ and $\bar{\boldsymbol{F}}''$. Let us introduce the following notation for their elements:

$$E[\boldsymbol{f}'\boldsymbol{f}'^T] \triangleq \begin{bmatrix} \phi_{11} & \phi_{12} \\ \phi_{21} & \phi_{22} \end{bmatrix} \quad \text{and}$$
$$\bar{\boldsymbol{F}}'' \triangleq \begin{bmatrix} \psi_{11} & \psi_{12} \\ \psi_{21} & \psi_{22} \end{bmatrix}. \quad (7)$$

For future use, we also define the following quantities, which depend only on the anchor coordinates:

$$X_a(\mathcal{A}) \triangleq \sum_{m=1}^{M} \frac{x_m^2}{x_m^2+y_m^2}, \quad X_b(\mathcal{A}) \triangleq \sum_{m=1}^{M} x_m^2,$$
$$Y_a(\mathcal{A}) \triangleq \sum_{m=1}^{M} \frac{y_m^2}{x_m^2+y_m^2}, \quad Y_b(\mathcal{A}) \triangleq \sum_{m=1}^{M} y_m^2,$$
$$Z_a(\mathcal{A}) \triangleq \sum_{m=1}^{M} \frac{x_m y_m}{x_m^2+y_m^2}, \quad Z_b(\mathcal{A}) \triangleq \sum_{m=1}^{M} x_m y_m,$$
$$X_c(\mathcal{A}) \triangleq \sum_{m=1}^{M} x_m^2(x_m^2+y_m^2),$$
$$Y_c(\mathcal{A}) \triangleq \sum_{m=1}^{M} y_m^2(x_m^2+y_m^2),$$
$$Z_c(\mathcal{A}) \triangleq \sum_{m=1}^{M} x_m y_m(x_m^2+y_m^2). \quad (8)$$

III. Asymptotic Accuracy of LS

LS works by minimizing (1) with respect to (x,y). With zero-mean white Gaussian noise, the performance of LS coincides with the CRB. See, e.g., [7, App. A] for the case of $N=1$. Hence, in principle, we could use well known formulas for its accuracy. However, a direct calculation from first principles is short, so we include it for completeness, and as a preparation for the analysis of SR-LS. Note that this calculation does not assume Gaussianity of the measurement noise.

We calculate the first partial derivatives as

$$\frac{\partial f}{\partial x}(0,0) = 2\sum_{m=1}^{M} \frac{e_m x_m}{\sqrt{x_m^2+y_m^2}} \quad \text{and}$$
$$\frac{\partial f}{\partial y}(0,0) = 2\sum_{m=1}^{M} \frac{e_m y_m}{\sqrt{x_m^2+y_m^2}}. \quad (9)$$

Equation (7) and (9) and the independence of e_m and e_n for $m \neq n$ give us the entries of $E[\boldsymbol{f}'\boldsymbol{f}'^T]$:

$$\phi_{11} = E\left[\left(\frac{\partial f}{\partial x}(0,0)\right)^2\right] = \frac{4\sigma^2}{N}\sum_{m=1}^{M}\frac{x_m^2}{x_m^2+y_m^2}$$
$$= \frac{4\sigma^2 X_a(\mathcal{A})}{N},$$
$$\phi_{22} = E\left[\left(\frac{\partial f}{\partial y}(0,0)\right)^2\right] = \frac{4\sigma^2}{N}\sum_{m=1}^{M}\frac{y_m^2}{x_m^2+y_m^2}$$
$$= \frac{4\sigma^2 Y_a(\mathcal{A})}{N},$$
$$\phi_{12} = \phi_{21} = E\left[\frac{\partial f}{\partial x}(0,0)\frac{\partial f}{\partial y}(0,0)\right]$$
$$= \frac{4\sigma^2}{N}\sum_{m=1}^{M}\frac{x_m y_m}{x_m^2+y_m^2} = \frac{4\sigma^2 Z_a(\mathcal{A})}{N}. \quad (10)$$

The second partial derivatives are calculated as

$$\frac{\partial^2 f}{\partial x^2}(0,0) = 2\sum_{m=1}^{M}\left(1 - \frac{r_m y_m^2}{(x_m^2+y_m^2)^{3/2}}\right),$$
$$\frac{\partial^2 f}{\partial x \partial y}(0,0) = 2\sum_{m=1}^{M}\frac{r_m x_m y_m}{(x_m^2+y_m^2)^{3/2}},$$
$$\frac{\partial^2 f}{\partial y^2}(0,0) = 2\sum_{m=1}^{M}\left(1 - \frac{r_m x_m^2}{(x_m^2+y_m^2)^{3/2}}\right). \quad (11)$$

Using (6), the entries of $\bar{\boldsymbol{F}}''$ follow as

$$\psi_{11} = \lim_{N\to\infty}\frac{\partial^2 f}{\partial x^2}(0,0)$$
$$= 2\sum_{m=1}^{M}\frac{x_m^2}{x_m^2+y_m^2} = 2X_a(\mathcal{A}),$$
$$\psi_{22} = \lim_{N\to\infty}\frac{\partial^2 f}{\partial y^2}(0,0)$$
$$= 2\sum_{m=1}^{M}\frac{y_m^2}{x_m^2+y_m^2} = 2Y_a(\mathcal{A}),$$
$$\psi_{12} = \psi_{21} = \lim_{N\to\infty}\frac{\partial^2 f}{\partial x \partial y}(0,0)$$
$$= 2\sum_{m=1}^{M}\frac{x_m y_m}{x_m^2+y_m^2} = 2Z_a(\mathcal{A}). \quad (12)$$

From (10) and (12), we observe that $E[\boldsymbol{f}'\boldsymbol{f}'^T] = 2\sigma^2\bar{\boldsymbol{F}}''/N$. Using (4), this gives the asymptotic (large N) error covariance matrix

$$\begin{aligned}\boldsymbol{Q}_{\mathrm{LS}} &= (\bar{\boldsymbol{F}}'')^{-1}E[\boldsymbol{f}'\boldsymbol{f}'^T](\bar{\boldsymbol{F}}'')^{-1} = \frac{2\sigma^2}{N}(\bar{\boldsymbol{F}}'')^{-1} \\ &= \frac{2\sigma^2}{N(\psi_{11}\psi_{22}-\psi_{12}\psi_{21})}\begin{bmatrix}\psi_{22} & -\psi_{12}\\ -\psi_{21} & \psi_{11}\end{bmatrix} \\ &= \frac{\sigma^2}{N(X_a(\mathcal{A})Y_a(\mathcal{A})-Z_a^2(\mathcal{A}))} \\ &\quad\times\begin{bmatrix}Y_a(\mathcal{A}) & -Z_a(\mathcal{A})\\ -Z_a(\mathcal{A}) & X_a(\mathcal{A})\end{bmatrix}. \end{aligned} \tag{13}$$

In particular, the mean-square error of the location estimate is

$$\begin{aligned}\mathrm{Tr}(\boldsymbol{Q}_{\mathrm{LS}}) &= Q_{11}+Q_{22} \\ &= \frac{\sigma^2(X_a(\mathcal{A})+Y_a(\mathcal{A}))}{N(X_a(\mathcal{A})Y_a(\mathcal{A})-Z_a^2(\mathcal{A}))} \\ &= \frac{\sigma^2}{N}\cdot\frac{M}{X_a(\mathcal{A})Y_a(\mathcal{A})-Z_a^2(\mathcal{A})}. \end{aligned} \tag{14}$$

IV. Asymptotic Accuracy of SR-LS

The SR-LS method estimates the position by minimizing (3). Here

$$\begin{aligned}\frac{\partial f}{\partial x}(0,0) &= 4\sum_{m=1}^{M}x_m\left(2e_m\sqrt{x_m^2+y_m^2}+e_m^2\right), \\ \frac{\partial f}{\partial y}(0,0) &= 4\sum_{m=1}^{M}y_m\left(2e_m\sqrt{x_m^2+y_m^2}+e_m^2\right), \\ \frac{\partial^2 f}{\partial x^2}(0,0) &= 4\sum_{m=1}^{M}[2x_m^2-(r_m^2-x_m^2-y_m^2)], \\ \frac{\partial^2 f}{\partial x\partial y}(0,0) &= 8\sum_{m=1}^{M}x_m y_m, \\ \frac{\partial^2 f}{\partial y^2}(0,0) &= 4\sum_{m=1}^{M}[2y_m^2-(r_m^2-x_m^2-y_m^2)]. \end{aligned} \tag{15}$$

With ϕ_{ij} and ψ_{ij} defined in (7), straightforward but tedious algebra gives (16), shown at the bottom of the page. Furthermore, since $r_m^2 \to x_m^2+y_m^2$ as $N\to\infty$ (cf. (6)), it follows that

$$\begin{aligned}\psi_{11} &= \lim_{N\to\infty}\frac{\partial^2 f}{\partial x^2}(0,0) = 8\sum_{m=1}^{M}x_m^2 = 8X_b(\mathcal{A}), \\ \psi_{22} &= \lim_{N\to\infty}\frac{\partial^2 f}{\partial y^2}(0,0) = 8\sum_{m=1}^{M}y_m^2 = 8Y_b(\mathcal{A}), \\ \psi_{12} &= \psi_{21} = \lim_{N\to\infty}\frac{\partial^2 f}{\partial x\partial y}(0,0) \\ &= 8\sum_{m=1}^{M}x_m y_m = 8Z_b(\mathcal{A}). \end{aligned} \tag{17}$$

The asymptotic (large N) error covariance matrix $\boldsymbol{Q}$ is given by (18), shown at the bottom of the next page, where we have used the facts that $\phi_{21}=\phi_{12}$ and $\psi_{21}=\psi_{12}$. For small σ^2/N (i.e., large N), we can neglect the terms which are $O(\sigma^4/N^2)$. The asymptotic mean-square error of the location estimate is given by (19), shown at the bottom of the next page.

V. Comparisons and Discussion

In this section, we will discuss the relation between the asymptotic accuracy of LS (14) and that of SR-LS (19). First note that the error covariance of SR-LS is always at least as large as that of LS. More precisely, $\boldsymbol{Q}_{\text{SR-LS}} \geq \boldsymbol{Q}_{\mathrm{LS}}$ (where the inequality $\boldsymbol{A}\geq\boldsymbol{B}$ means that $\boldsymbol{A}-\boldsymbol{B}$ is positive semidefinite), and especially, $\mathrm{Tr}(\boldsymbol{Q}_{\text{SR-LS}}) \geq \mathrm{Tr}(\boldsymbol{Q}_{\mathrm{LS}})$. This

$$\begin{aligned}\phi_{11} &= E\left[\left(\frac{\partial f}{\partial x}(0,0)\right)^2\right] \\ &= \frac{16\sigma^2}{N}\left(4\sum_{m=1}^{M}x_m^2(x_m^2+y_m^2)+\frac{\sigma^2}{N}\left(\sum_{m=1}^{M}x_m\right)^2+\frac{\sigma^2}{N}\left(2+\frac{\alpha-3}{N}\right)\sum_{m=1}^{M}x_m^2\right) \\ &= \frac{64\sigma^2}{N}X_c(\mathcal{A})+\frac{16\sigma^4}{N^2}\left[\left(\sum_{m=1}^{M}x_m\right)^2+2X_b(\mathcal{A})\right]+\frac{16(\alpha-3)\sigma^4}{N^3}X_b(\mathcal{A}), \\ \phi_{22} &= E\left[\left(\frac{\partial f}{\partial y}(0,0)\right)^2\right] \\ &= \frac{16\sigma^2}{N}\left(4\sum_{m=1}^{M}y_m^2(x_m^2+y_m^2)+\frac{\sigma^2}{N}\left(\sum_{m=1}^{M}y_m\right)^2+\frac{\sigma^2}{N}\left(2+\frac{\alpha-3}{N}\right)\sum_{m=1}^{M}y_m^2\right) \\ &= \frac{64\sigma^2}{N}Y_c(\mathcal{A})+\frac{16\sigma^4}{N^2}\left[\left(\sum_{m=1}^{M}y_m\right)^2+2Y_b(\mathcal{A})\right]+\frac{16(\alpha-3)\sigma^4}{N^3}Y_b(\mathcal{A}), \\ \phi_{12} &= \phi_{21} = E\left[\frac{\partial f}{\partial x}(0,0)\frac{\partial f}{\partial y}(0,0)\right] \\ &= \frac{16\sigma^2}{N}\left(4\sum_{m=1}^{M}x_m y_m(x_m^2+y_m^2)+\frac{\sigma^2}{N}\left(\sum_{m=1}^{M}x_m\right)\left(\sum_{m=1}^{M}y_m\right)+\left(2+\frac{\alpha-3}{N}\right)\sum_{m=1}^{M}x_m y_m\right) \\ &= \frac{64\sigma^2}{N}Z_c(\mathcal{A})+\frac{16\sigma^4}{N^2}\left[\left(\sum_{m=1}^{M}x_m\right)\left(\sum_{m=1}^{M}y_m\right)+2Z_b(\mathcal{A})\right]+\frac{16(\alpha-3)\sigma^4}{N^3}Z_b(\mathcal{A}). \end{aligned} \tag{16}$$

follows since $\boldsymbol{Q}_{\mathrm{LS}}$ coincides with the CRB on the achievable accuracy in Gaussian noise; hence no other estimator can have a smaller error covariance matrix so we must have $\boldsymbol{Q}_{\text{SR-LS}} \geq \boldsymbol{Q}_{\mathrm{LS}}$. In addition, for LS, adding an extra anchor to a given geometry always improves accuracy, because new information is added and the CRB therefore decreases. For SR-LS, this is not necessarily so. Special case 4 below exemplifies this point. There, $\mathrm{Tr}(\boldsymbol{Q}_{\text{SR-LS}})$ is finite if only the first two anchors are used. However, when using all three anchors, we have that $\mathrm{Tr}(\boldsymbol{Q}_{\text{SR-LS}}) \to \infty$ as the third anchor moves away from the source ($p \to \infty$).

Accurate localization is more difficult for some geometries than for others. The "difficulty" of a specific geometry can be quantified in terms of its geometric dilution of precision, defined as $\mathrm{GDOP} \triangleq N/\sigma^2 \cdot \mathrm{Tr}(\boldsymbol{Q})$. The GDOP essentially relates position accuracy to the measurement accuracy. We have that $X_a(\mathcal{A})Y_a(\mathcal{A}) > Z_a^2(\mathcal{A})$ and $X_b(\mathcal{A})Y_b(\mathcal{A}) > Z_b^2(\mathcal{A})$ unless $\mathcal{A}$ lie on a straight line through $(0,0)$.[3] Hence, excluding such degenerate geometries, the denominators of (14) and (19) are nonzero (and $\bar{\boldsymbol{F}}''$ is nonsingular), and $\boldsymbol{Q}$ is finite for both LS and SR-LS.

What geometries have a large GDOP? For LS, it is clear that the GDOP is large if $X_a(\mathcal{A})Y_a(\mathcal{A}) \approx Z_a^2(\mathcal{A})$ so that the denominator of (14) is small. That happens if $\mathcal{A}$ nearly lie on a straight line through $(0,0)$. For SR-LS, matters are much more involved and there appears to be no simple, universal answer. However, we can give the following argument. Introduce polar coordinates (d_m, β_m) for the locations of $\mathcal{A}$, so that $x_m = d_m \cos(\beta_m)$ and $y_m = d_m \sin(\beta_m)$ for $m = 1, \ldots, M$. Denote the numerator and denominator of (19) with η and ξ, so that $\mathrm{Tr}(\boldsymbol{Q}_{\text{SR-LS}}) = \sigma^2/N \cdot \eta/\xi$. We have

$$\xi \triangleq \left(\left(\sum_{m=1}^{M} d_m^2 \cos^2(\beta_m)\right)\left(\sum_{m=1}^{M} d_m^2 \sin^2(\beta_m)\right) - \left(\sum_{m=1}^{M} d_m^2 \cos(\beta_m)\sin(\beta_m)\right)^2\right)^2.$$

[3]To see this, note that by the Cauchy–Schwartz inequality,

$$\left(\sum_{m=1}^{M} x_m y_m / x_m^2 + y_m^2\right)^2 \leq \left(\sum_{m=1}^{M} x_m^2/x_m^2 + y_m^2\right)\left(\sum_{m=1}^{M} y_m^2/x_m^2 + y_m^2\right)$$

with equality precisely when $\mathcal{A}$ lie on a line through $(0,0)$. Likewise,

$$\left(\sum_{m=1}^{M} x_m y_m\right)^2 \leq \left(\sum_{m=1}^{M} x_m^2\right)\left(\sum_{m=1}^{M} y_m^2\right)$$

with equality under the same condition.

Both η and ξ are $O(d_m^8)$. One situation where we can expect accuracy to be poor is when ξ is small relative to η. Generally, the behavior of ξ is dominated by the terms in it for which d_m is large. Large d_m correspond to anchors far from $(0,0)$. Suppose the anchors which are far from $(0,0)$ (have large d_m) lie nearly on a straight line through the origin. Then ξ will be small, relative to its value for other anchor constellations with the same d_m. Hence, one (but probably not the only) case when we may expect poor accuracy for SR-LS is geometries where d_m are very different and β_m are unluckily chosen.

To get some insight, we next study a few specially constructed geometries (see Fig. 1 and Table I) and some random geometries. Before we proceed we note that we can rotate the anchor coordinates by an arbitrary angle, without changing the mean-square errors. This is so because rotating the coordinate system amounts to multiplying the error covariance matrix by an orthonormal matrix, and this does not change its trace. The same invariance holds if all anchor coordinates are scaled by a constant; the error variance remains unchanged then too. This is immediate from (14) and (19). Thus, when studying interesting special geometries, we can assume without loss of generality that $\mathcal{A}_1 = (1,0)$.

1) Special Case 1 [Fig. 1(a)]: $\|\mathcal{A}_m\| = R$ for all m. In this example all anchors are located on a circle, with radius R say, centered at $\mathcal{S}$. Here, the performances of LS and SR-LS coincide:

$$\mathrm{Tr}(\boldsymbol{Q}_{\mathrm{LS}}) = \mathrm{Tr}(\boldsymbol{Q}_{\text{SR-LS}}) = \frac{\sigma^2}{N} \cdot \frac{M}{X_a(\mathcal{A})Y_a(\mathcal{A}) - Z_a^2(\mathcal{A})}.$$

The variance is finite unless all anchors lie on a straight line through the origin.

2) Special Case 2 [Fig. 1(b)]: $M = 3$ and $\mathcal{A}_1 = -\mathcal{A}_2$. In this special case we have two anchors in an "antipodal" configuration, and a third anchor at an arbitrary position. More precisely, $\mathcal{A}_1 = (1,0)$, $\mathcal{A}_2 = (-1,0)$ and $\mathcal{A}_3 = (p,q)$. The performances are equal here as well:

$$\mathrm{Tr}(\boldsymbol{Q}_{\mathrm{LS}}) = \mathrm{Tr}(\boldsymbol{Q}_{\text{SR-LS}}) = \frac{\sigma^2}{N} \cdot \frac{3(p^2+q^2)}{2q^2}.$$

This variance is finite unless $q \to 0$, that is, the third anchor must not lie on the horizontal axis.

3) Special Case 3 [Fig. 1(c)]: $M = 3$, $\mathcal{A}_1 \perp \mathcal{A}_2$ and $\|\mathcal{A}_1\| = \|\mathcal{A}_2\|$. In this example, $\mathcal{A}_1 = (1,0)$, $\mathcal{A}_2 = (0,1)$ and $\mathcal{A}_3 = (p,q)$.

$$\begin{aligned}
\boldsymbol{Q}_{\text{SR-LS}} &= (\bar{\boldsymbol{F}}'')^{-1} E[\boldsymbol{f}'\boldsymbol{f}'^T](\bar{\boldsymbol{F}}'')^{-1} \\
&= \frac{1}{(\psi_{11}\psi_{22} - \psi_{12}^2)^2} \times \begin{bmatrix} \psi_{22} & -\psi_{12} \\ -\psi_{21} & \psi_{11} \end{bmatrix} \times \begin{bmatrix} \phi_{11} & \phi_{12} \\ \phi_{21} & \phi_{22} \end{bmatrix} \times \begin{bmatrix} \psi_{22} & -\psi_{12} \\ -\psi_{21} & \psi_{11} \end{bmatrix} \\
&= \frac{1}{(\psi_{11}\psi_{22} - \psi_{12}^2)^2} \\
&\quad \times \begin{bmatrix} \phi_{11}\psi_{22}^2 + \phi_{22}\psi_{12}^2 - 2\phi_{12}\psi_{12}\psi_{22} & \phi_{12}(\psi_{12}^2 + \psi_{11}\psi_{22}) - \psi_{12}(\phi_{11}\psi_{22} + \phi_{22}\psi_{11}) \\ \phi_{12}(\psi_{12}^2 + \psi_{11}\psi_{22}) - \psi_{12}(\phi_{11}\psi_{22} + \phi_{22}\psi_{11}) & \phi_{11}\psi_{12}^2 + \phi_{22}\psi_{11}^2 - 2\phi_{12}\psi_{12}\psi_{11} \end{bmatrix}
\end{aligned} \tag{18}$$

$$\begin{aligned}
\mathrm{Tr}(Q_{\text{SR-LS}}) &= Q_{11} + Q_{22} = \frac{(\phi_{11}+\phi_{22})\psi_{12}^2 - 2\phi_{12}\psi_{12}(\psi_{11}+\psi_{22}) + \phi_{11}\psi_{22}^2 + \phi_{22}\psi_{11}^2}{(\psi_{11}\psi_{22} - \psi_{12}\psi_{21})^2} \\
&= \frac{\sigma^2}{N} \cdot \frac{Z_b^2(\mathcal{A})(X_c(\mathcal{A}) + Y_c(\mathcal{A})) - 2Z_c(\mathcal{A})Z_b(\mathcal{A})(X_b(\mathcal{A}) + Y_b(\mathcal{A})) + X_c(\mathcal{A})Y_b^2(\mathcal{A}) + Y_c(\mathcal{A})X_b^2(\mathcal{A})}{(X_b(\mathcal{A})Y_b(\mathcal{A}) - Z_b^2(\mathcal{A}))^2}
\end{aligned} \tag{19}$$

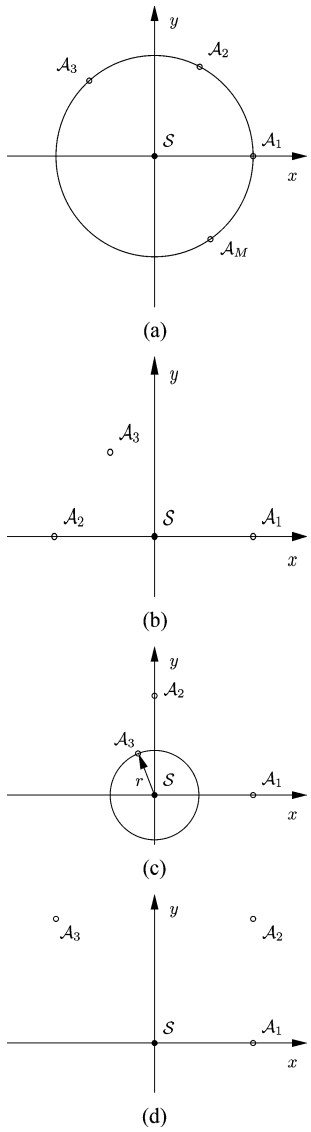

Fig. 1. Four special geometries of interest. (a) Special case 1: All anchors on a circle centered at $\mathcal{S}$. (b) Special case 2: Two anchors in "antipodal configuration", and a third anchor at an arbitrary position. (c) Special case 3: Example of a geometry where LS and SR-LS perform differently. (d) Special case 4: Example of a geometry with unbounded performance difference.

In this case the performances of LS and SR-LS differ. The relation between the asymptotic mean-square errors is

$$\Delta \triangleq \frac{\mathrm{Tr}(\boldsymbol{Q}_{\text{SR-LS}})}{\mathrm{Tr}(\boldsymbol{Q}_{\text{LS}})} = \frac{4}{3}\left(1 - \left(\frac{r}{1+r^2}\right)^2\right) \tag{20}$$

where $r = \sqrt{p^2+q^2}$. Fig. 2 shows the standard deviation ratio $\sqrt{\Delta}$ as a function of the distance $\sqrt{p^2+q^2}$ from $\mathcal{A}_3$ to $\mathcal{S}$. Clearly, the difference is bounded but it can be substantial (up to 15% in error standard deviation). The difference vanishes precisely if $r = 1$; then we have special case 2 above.

4) Special Case 4 [Fig. 1(d)]: $M = 3$. In this example we provide an anchor constellation for which the difference in the performance of the SR-LS and LS algorithms is *unbounded*. This constellation consists of the anchors at locations $\mathcal{A}_1 = (1,0)$, $\mathcal{A}_2 = (1,p)$ and $\mathcal{A}_3 = (-1,p)$. Here

$$\Delta = \frac{\mathrm{Tr}(\boldsymbol{Q}_{\text{SR-LS}})}{\mathrm{Tr}(\boldsymbol{Q}_{\text{LS}})} = \frac{(p^2+3)^2(4p^2+3)}{27(p^2+1)^2}.$$

TABLE I
THE QUANTITIES IN (8) THAT ARE NEEDED TO EVALUATE (14) AND (19), FOR THE FOUR SPECIAL CASES OF FIG. 1

Case	$X_a(\mathcal{A})$	$X_b(\mathcal{A})$	$X_c(\mathcal{A})$
1	$\frac{1}{R^2}\sum_{m=1}^M x_m^2$	$\sum_{m=1}^M x_m^2$	$R^2\sum_{m=1}^M x_m^2$
2	$2+\frac{p^2}{p^2+q^2}$	$2+p^2$	$2+p^2(p^2+q^2)$
3	$1+\frac{p^2}{p^2+q^2}$	$1+p^2$	$1+p^2(p^2+q^2)$
4	$1+\frac{2}{1+p^2}$	3	$3+2p^2$
Case	$Y_a(\mathcal{A})$	$Y_b(\mathcal{A})$	$Y_c(\mathcal{A})$
1	$\frac{1}{R^2}\sum_{m=1}^M y_m^2$	$\sum_{m=1}^M y_m^2$	$R^2\sum_{m=1}^M y_m^2$
2	$\frac{q^2}{p^2+q^2}$	q^2	$q^2(p^2+q^2)$
3	$1+\frac{q^2}{p^2+q^2}$	$1+q^2$	$1+q^2(p^2+q^2)$
4	$\frac{2p^2}{1+p^2}$	$2p^2$	$2p^2(1+p^2)$
Case	$Z_a(\mathcal{A})$	$Z_b(\mathcal{A})$	$Z_c(\mathcal{A})$
1	$\frac{1}{R^2}\sum_{m=1}^M x_m y_m$	$\sum_{m=1}^M x_m y_m$	$R^2\sum_{m=1}^M x_m y_m$
2	$\frac{pq}{p^2+q^2}$	pq	$pq(p^2+q^2)$
3	$\frac{pq}{p^2+q^2}$	pq	$pq(p^2+q^2)$
4	0	0	0

For example, for $p = 10$, which hardly represents an extreme measurement geometry, LS is four times more accurate than SR-LS: $\sqrt{\Delta} \approx 4$. More importantly, if we let $p \to \infty$, then $\Delta \to \infty$. This shows that we cannot upper bound the difference in performance of the two algorithms. Note that

$$\mathrm{Tr}(\boldsymbol{Q}_{\text{LS}}) = \frac{\sigma^2}{N}\cdot\frac{3(p^2+1)^2}{2p^2(p^2+3)} \le \frac{3}{2}\cdot\frac{\sigma^2}{N}.$$

for $p \ge 1$. Therefore, this geometry is not "bad" for LS, not even if p is very large.

Note that the somewhat similar geometry $\mathcal{A}_1 = (1,0)$, $\mathcal{A}_2 = (1,p)$ and $\mathcal{A}_3 = (-1,-p)$ is not a bad geometry for SR-LS even as $p \to \infty$. Indeed, this geometry is special case 2.

5) Random Geometries: To get a feeling for the *average* asymptotic performance difference between LS and SR-LS, we evaluated Δ numerically for a large number of random geometries. Specifically, we placed M anchors uniformly at random inside a disk of unit radius centered at $\mathcal{S}$. The choice of the disk radius is unimportant since the performances of both LS and SR-LS are invariant to a scaling of the geometry. Fig. 3 shows empirical probability density functions for $\sqrt{\Delta}$ for different numbers of anchors M. From Fig. 3, we see that for a large number of anchors, the performance loss of SR-LS relative to LS tends to concentrate around 15%.

We next study the percentiles of $\sqrt{\Delta}$ for the random geometry setup explained above. Fig. 4 shows the 99% and 50% percentiles of $\sqrt{\Delta}$ for three different situations.

i) *Random geometry*. Here the anchors are placed uniformly at random within the unit disk.
ii) *90% best geometries*. Here we consider only the 90% of the geometries for which $\mathrm{Tr}(\boldsymbol{Q}_{\text{LS}})$ is lowest. That is, we exclude the 10% most difficult geometries for LS.
iii) *90% closest anchor farthest away*. Here we consider the 90% of the geometries with the largest

$$d_{\min} \triangleq \min_{m\in[1,\ldots,M]} d_m.$$

That is, we exclude the 10% of the geometries where one or more anchors are very close to $\mathcal{S}$.

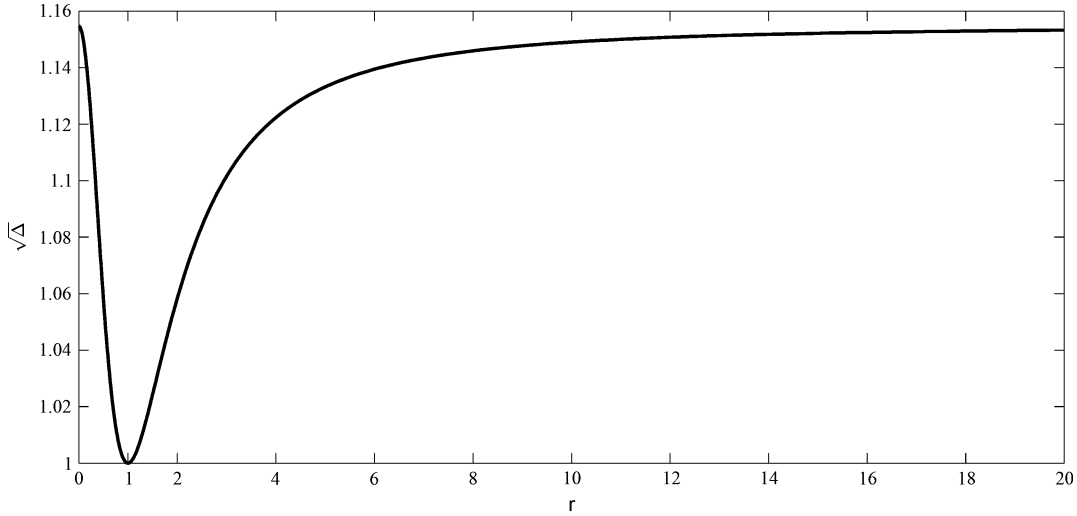

Fig. 2. Ratio of the standard error deviations for special case 3.

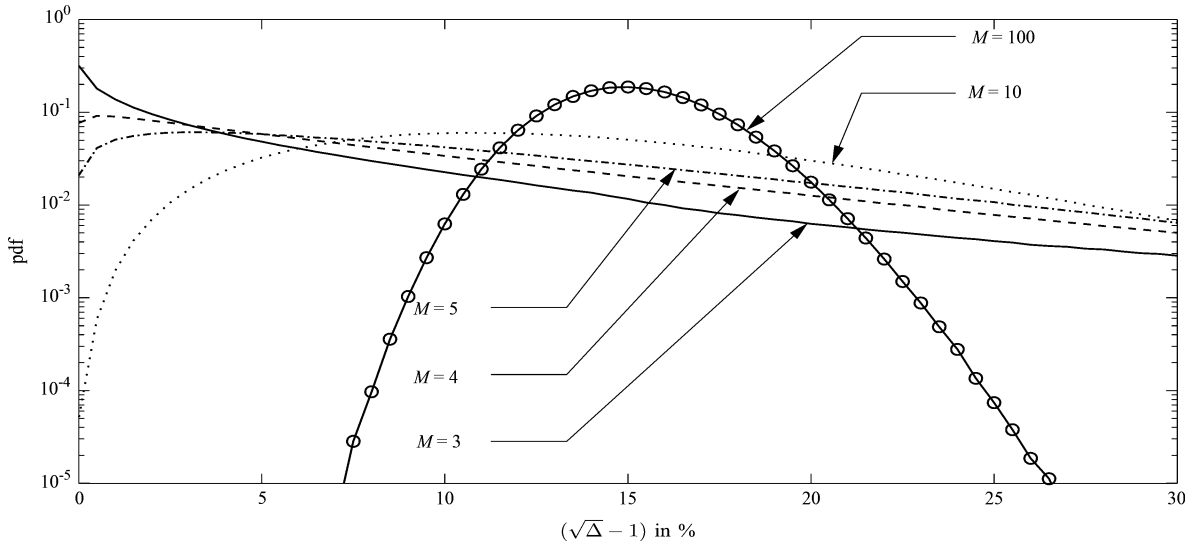

Fig. 3. Empirical probability density functions of the asymptotic performance ratio $\sqrt{\Delta}$, for different numbers of anchors M.

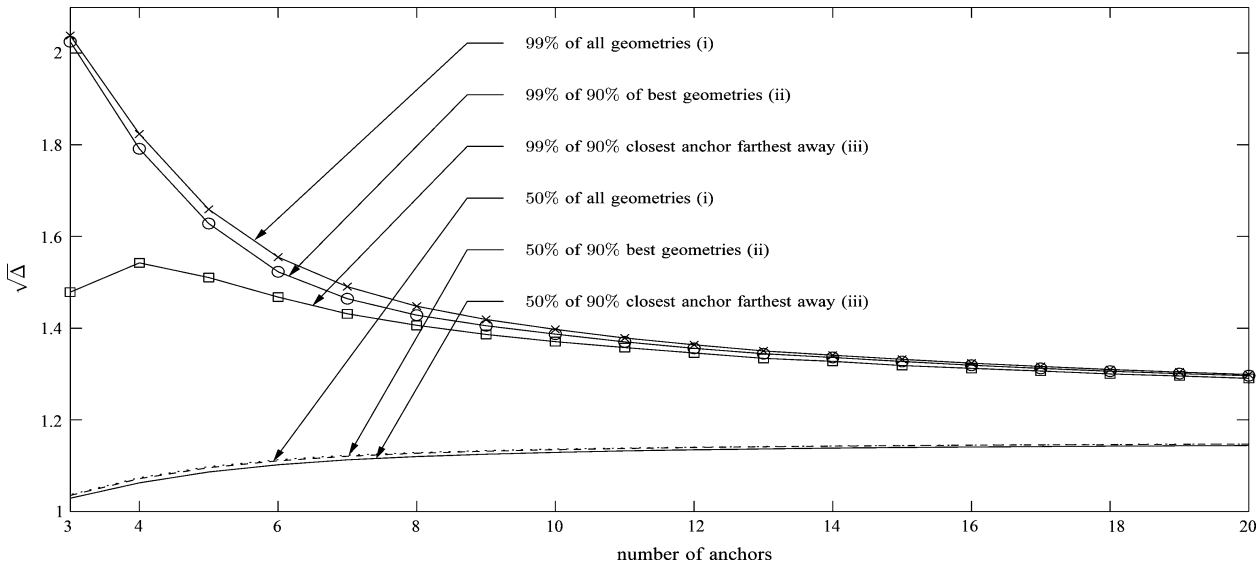

Fig. 4. Percentile values of $\sqrt{\Delta}$ for the SR-LS and LS algorithms in different situations.

For the 50% percentiles (median) the graphs are nearly the same so the median of $\sqrt{\Delta}$ is not significantly affected by the potentially difficult geometries that we exclude in ii) and iii). The 99% percentile is nearly the same for cases i) and ii), but much lower for case iii).

To summarize, the performances of LS and SR-LS differ in general. The simulations and discussion here suggest that the worst-case performance ratio $\sqrt{\Delta}$ can be larger if the ranges $d_1, \ldots, d_M$ span a large range. While we believe that the examples and discussion here give substantial insight, we must state the complete characterization of bad geometries for SR-LS as an open problem.

VI. Conclusion

Compared to classical LS, SR-LS [1] is a computationally very attractive approach to the source localization problem, since it can find the global minimum of the cost function without resorting to heuristic divide-and-conquer methods or heuristic techniques for solving nonconvex optimization problems. We have computed and compared the asymptotic accuracies of LS and SR-LS. Our main observations are i) there exist geometries, where LS and SR-LS have identical performances and ii) there are geometries, for which the difference in performance between LS and SR-LS is unbounded. We also exemplified the asymptotic performance difference numerically for random geometries. Taken together, SR-LS performs well relative to LS for most geometries, but not for all. If SR-LS is used in practice, then care should be taken to avoid the geometries that the method has difficulties with. If the position of $\mathcal{S}$ is approximately known *a priori*, then the achievable accuracy can be estimated by using (14) and (19), before choosing what localization algorithm to use.

The numerical results presented in this paper are reproducible. To obtain the relevant MATLAB programs go to www.commsys.isy.liu.se/~egl/rr . Included therein is also Monte Carlo simulation code for numerically verifying the validity of the asymptotic accuracy formulas that we derived.

References

[1] A. Beck, P. Stoica, and J. Li, "Exact and approximate solutions of source localization problems," *IEEE Trans. Signal Process.*, vol. 56, no. 5, pp. 1770–1778, May 2008.

[2] *Global Positioning System: Theory and Applications*, ser. Progress in Astronautics and Aeronautics, B. Parkinson and J. Spilker, Jr., Eds. Washington, DC: Amer. Instit. Aeronautics Astronautics, 1996, vol. 163.

[3] J. Caffery, Jr. and G. Stüber, "Subscriber location in CDMA cellular networks," *IEEE Trans. Veh. Technol.*, vol. 47, pp. 406–416, May 1998.

[4] G. Sun, J. Chen, W. Guo, and K. Liu, "Signal processing techniques in network-aided positioning: A survey of state-of-the-art positioning designs," *IEEE Signal Process. Mag.*, vol. 22, no. 4, pp. 12–23, Jul. 2005.

[5] K.-F. Ssu, C.-H. Ou, and H. Jiau, "Localization with mobile anchor points in wireless sensor networks," *IEEE Trans. Veh. Technol.*, vol. 54, pp. 1187–1197, May 2005.

[6] S. M. Kay, *Fundamentals of Statistical Signal Processing: Estimation Theory*. Englewood Cliffs, NJ: Prentice-Hall, 1993.

[7] K. Cheung, H. So, W.-K. Ma, and Y. Chan, "Least squares algorithms for time-of-arrival-based mobile location," *IEEE Trans. Signal Process.*, vol. 52, no. 4, pp. 1121–1130, Apr. 2004.

[8] L. Ljung, *System Identification: Theory for the User*, 2nd ed. Englewood Cliffs, NJ: Prentice-Hall, 1998.

[9] M. Viberg and B. Ottersten, "Sensor array processing based on subspace fitting," *IEEE Trans. Signal Process.*, vol. 39, no. 5, pp. 1110–1121, May 1991.

[10] P. Stoica and T. Söderström, *System Identification*. Englewood Cliffs, NJ: Prentice-Hall, 1989.

[11] A. Papoulis, *Probability, Random Variables, and Stochastic Processes*, 3rd ed. New York: McGraw-Hill, 1991.

Efficient Estimation of a Narrow-Band Polynomial Phase Signal Impinging on a Sensor Array

Alon Amar

***Abstract*—The parameters of interest of a polynomial phase signal observed by a sensor array include the direction of arrival and the polynomial coefficients. The direct maximum likelihood estimation of these parameters requires a nonlinear multidimensional search. In this paper, we present a two-step estimation approach. The estimation requires only a one-dimensional search in the direction of arrival space and involves a simple least squares solution for the polynomial coefficients. The efficiency of the estimates is corroborated by Monte Carlo simulations.**

***Index Terms*—Extended invariance property, maximum likelihood estimation, polynomial phase signal.**

I. Introduction

Polynomial phase signals (PPSs) attract attention in radar, sonar, and communications systems. Previous research has considered PPSs observed with a single sensor [1]–[5] and also with a sensor array [6]–[10]. We focus on the latter case here. The parameters of interest are the direction of arrival (DOA) and the polynomial coefficients of the signal's phase.

The maximum likelihood estimator (MLE) requires a large amount of computation since it involves the maximization of a multivariable cost function and is therefore not practically useful. For example, the MLE in [6] extracts the parameters of a chirp signal (PPS of order two) with a three-dimensional search in the DOA, frequency, and frequency-rate spaces.

The goal of this paper is to suggest an efficient parameter estimation of a single narrow-band PPS impinging on an array, based on the extended invariance property (EXIP) [11]. It is shown that the DOA is estimated by a one-dimensional search and that the polynomial coefficients are obtained by a simple least squares (LS) solution. Simulation results corroborate that the estimates asymptotically converge to the Cramér–Rao lower bound (CRLB) at high signal-to-noise ratio (SNR).

II. Problem Formulation

Consider a uniform linear array (ULA) composed of M sensors. Assume that the transmitted signal can be modeled as $\tilde{s}(t;\alpha,\mathbf{b}) \triangleq \alpha e^{j\tilde{\phi}(t;\mathbf{b})}$, where α is the unknown amplitude, $\tilde{\phi}(t;\mathbf{b}) = \omega_0 t + \phi(t;\mathbf{b})$, where ω_0 is the carrier frequency, and $\phi(t;\mathbf{b}) \triangleq \mathbf{b}^T\mathbf{u}(t)$ with $\mathbf{u}(t) \triangleq [1, t, \ldots, t^P]^T$, P is the known polynomial order, and $\mathbf{b} \triangleq [b_0, b_1, \ldots, b_P]^T$ is the vector of polynomial coefficients. The noiseless signal observed at the mth element of the array over the time interval $T_0 \le t \le T_0 + T$ is $\tilde{x}_m(t) = (\alpha/\sqrt{M})e^{j\tilde{\phi}(t+\tau_m;\mathbf{b})}$, $m = 1, \ldots, M$, where $\tau_m = (d/c)(m-1)\sin(\theta)$, θ is the signal's DOA, c is the propagation speed of the signal, and d is the interelement spacing. According to the mean value theorem of Lagrange, we can write

Manuscript received March 08, 2009; accepted July 17, 2009. First published August 18, 2009; current version published January 13, 2010. The associate editor coordinating the review of this manuscript and approving it for publication was Prof. Antonio Napolitano. This work was supported in part by NWO-STW under the VICI program (DTC.5893).

The author is with the Circuits and Systems Group, Faculty of Electrical Engineering, Mathematics and Computer Science, Delft University of Technology, Delft 2628 CD, The Netherlands (e-mail: a.amar@tudelft.nl).

Digital Object Identifier 10.1109/TSP.2009.2030608